First-principles calculations of energetics and electronic structure for reconstructed Si(111)-(5 × *n*)-Au surfaces

K. Seino* and F. Bechstedt

Institut für Festkörpertheorie und -optik, Friedrich-Schiller-Universität Jena, Max-Wien-Platz 1, 07743 Jena, Germany

(Received 27 May 2014; published 6 October 2014)

We report results of *ab initio* calculations with various exchange-correlation functionals for the Si(111) surface with a 0.6-monolayer Au decoration. Seven different variations of the recently developed Erwin-Barke-Himpsel and Abukawa-Nishigaya models are studied in detail. Atomic geometries are determined by total-energy minimizations. We find the Erwin-Barke-Himpsel model of the Si(111)-(5 × 4)-Au surface with one Si adatom per unit cell to be the most favorable structure. Seven-member rings and undercoordinated Si atoms of the Abukawa-Nishigaya model are unstable. Scanning tunneling images and band structures are calculated for the controversial geometries. For the (5 × 4) adatom geometry the resulting electronic structure agrees with the available experimental data.

DOI: 10.1103/PhysRevB.90.165407 PACS number(s): 68.35.Md, 68.43.Fg, 73.20.At, 71.15.Nc

I. INTRODUCTION

In recent years Au/Si(111) surfaces have become fascinating due to the formation of reconstructions that are, at least structurally, quasi-one-dimensional (quasi-1D) due to the formation of chainlike structure motifs. Many of the reconstructions consist of parallel arrangements of Si chains that are separated by wires of Au atoms. One of the most common Au-induced surface phases, the 5 × 2 reconstruction, has been widely studied as a prototype metallic chain array system in which elements of the 1D physics seem to be realized [1,2]. There are some indications that the mechanism for electronic instabilities or even Luttinger-liquid physics may be observable [3].

Despite more than 40 years of intensive experimental and theoretical research [3], the atomic geometry and the corresponding electronic properties of the Si(111)-(5 × 2)-Au system are still not settled. The first observation of a fivefold periodicity in the Au-decorated Si(111) surface, such as in Si(111)-(5 × 2)-Au, was made in 1969 by means of low-energy electron diffraction (LEED) and Auger emission spectroscopy [4]. In 2009 a recalibration of the Au coverage from 0.4 monolayer (ML) to 0.6 ML was found for the 5×2 reconstruction [5]. These findings prompted a reevaluation of the Si(111)-(5×2)-Au surface since the structural models proposed for the 0.4-ML coverage [6–8] are invalid. Based on total-energy calculations within the density-functional theory (DFT), scanning tunneling microscopy (STM), and angle-resolved photoemission spectroscopy (ARPES) experiments, Erwin, Barke, and Himpsel (EBH) proposed a structural model [9]. This three-chain model with a narrow stripe of a Si honeycomb chain (Si HC), a Au double row (Au D), and a Au single row (Au S) was claimed to explain all available experimental data. However, very recently, based on their reflection high-energy electron diffraction (RHEED) data, Abukawa and Nishigaya (AN) predicted a completely different geometry with Au dimers but without Si honeycomb chains [10]. The structural motifs are explained to be consistent with the Y-shaped STM images [11,12]. Results from recent reflectance anisotropy spectroscopy (RAS) and first-principles studies, however, seem to support the EBH model [13]. Therefore, the two controversial structural models of the Si(111)-(5×2)-Au surface, EBH and AN, require further discriminating studies.

The majority of the previous DFT calculations were performed for a Au coverage of 0.4 ML [6–8]. A detailed comparison of theoretical results for the variation of the EBH and AN models is missing. Therefore, in this paper, we study these two basic models, which differ with respect to the arrangement of the same number of Au atoms in rows or "towerlike" structures in the framework of the *ab initio* DFT. The role of Si adatoms is also studied. For the atomic geometries we test the influence of various modifications of the exchange-correlation functional, including the effect of dispersion forces. In addition to the energetics and the atomic geometries, the resulting electronic structures, i.e., surface bands and STM images, are presented. An extensive comparison of our results with available experimental and theoretical results closes the paper.

II. COMPUTATIONAL METHODS

A. Total-energy calculations

First-principles calculations are used to determine equilibrium geometries and surface energies of the basic reconstruction models and their variations. The calculations are performed in the framework of the DFT [14,15] using the Vienna Ab initio Simulation Package (VASP) implementation [16]. Exchange and correlation are treated within the local-density approximation (LDA) according to Perdew and Zunger [17] or a semilocal density treatment within the generalized gradient approximation (GGA) introduced by Perdew, Burke, and Ernzerhof (PBE) [18]. From previous calculations [19] we know that neither the LDA nor the GGA leads simultaneously to reasonable results for the lattice constants and cohesive energies of bulk gold and the group-IV crystals (see also Table I). The theoretical lattice constants underestimate the experimental values for LDA or overestimate them for PBE. Therefore, here we also test a modern GGA functional, PBEsol [20], which is intended for only solid and surface

*seino@ifto.physik.uni-jena.de

 ©2014 American Physical Society

TABLE I. Cubic lattice constant a_0 (in Å) and bulk modulus B_0 (in GPa) calculated by means of different XC functionals (see text). For comparison, experimental values are taken from the collection in Ref. [25].

	Au		Si	
XC functional	a_0	B_0	a_0	B_0
LDA	4.06	191	5.40	96.5
PBE-GGA	4.17	137	5.47	88.8
PBEsol	4.10	171	5.44	93.6
vdW-DF	4.14	153	5.46	90.9
Expt.	4.08	166–171	5.43	99.2

systems, and the van der Waals density functional (vdW-DF) [21,22] method, which is an exchange-correlation (XC) functional that includes vdW interaction and performs better for semiconductors and metals. The dispersion forces are approximated according to Dion *et al.* [21]. The details of the vdW-DF method are described by Klimeš *et al.* [22]. The correlation in the LDA is corrected by the dispersion effects. The exchange functional in GGA is used in the optB86b setting (see Ref. [22]).

The pseudopotentials and the wave function in the core region are generated within the projected-augmented wave (PAW) method [23]. The electronic wave functions are expanded into plane waves up to an energy cutoff of 400 eV. For the Brillouin-zone (BZ) integrations, $20 \times 20 \times 20$ and $10 \times 10 \times 10$ meshes of the Monkhorst-Pack (MP) type [24] were used in the case of bulk Au and Si, respectively. The results for bulk Au and Si crystallizing in a fcc or diamond structure are listed in Table I. They show the typical underestimation (overestimation) of the experimental lattice constant a_0 using the LDA (PBE-GGA) functional. The opposite tendency is observed for the bulk modulus B_0. The best agreement between theory and experiment occurs for the PBEsol XC functional. The values of a_0 and B_0 for Si bulk predicted by vdW-DF are consistent with the previous calculations [22]. The vdW-DF results agree somewhat better with experiment than the PBE ones. However, the tendency for overestimation of the bond lengths but underestimation of the elastic coefficients is still observable. We conclude that for compact systems the PBEsol functional should be applied. Nevertheless, we will also study the more open surface systems within the vdW-DF method to describe correctly the bonding of more distant atoms.

B. Surface modeling

The gold-covered Si(111) surfaces are simulated by repeated slabs of six double (i.e., 12 atomic) layers of Si atoms separated by a vacuum region of the same extent, i.e., by about 19 Å. The bottom layer of the slab is saturated with H atoms. The top side is decorated by 0.6 ML of gold. Additional Si atoms, i.e., adatoms, are sometimes allowed. This leads to 5×1, 5×2, or 5×4 surface reconstructions. The **k** summations are performed using $2 \times 8 \times 1$, $2 \times 4 \times 1$, and $2 \times 2 \times 1$ MP meshes, respectively. The four topmost Si bilayers, Si adatoms, and Au atoms are allowed to relax until the Hellmann-Feynman forces are less than 10 meV/Å.

In principle, a variety of surface geometries with varying numbers of Au atoms (N_{Au}) and of Si atoms (N_{Si}) has to be evaluated energetically and hence optimized structurally. This fact suggests to study the Planck's grand canonical thermodynamic potential. More precisely, we compare surface formation energies (per surface unit cell of a given slab) of the form [26]

$$\Omega_f = E_{\mathrm{slab}}(N_{\mathrm{Si}}, N_{\mathrm{Au}}, N_{\mathrm{H}}) - \mu_{\mathrm{Si}} N_{\mathrm{Si}} - \mu_{\mathrm{Au}} N_{\mathrm{Au}} - \mu_{\mathrm{H}} N_{\mathrm{H}}, \tag{1}$$

where E_{slab} is the total energy of the slab containing N_{Si} Si atoms, N_{Au} Au atoms, and N_{H} H atoms and μ_{Si}, μ_{Au}, and μ_{H} are the chemical potentials of the Si, Au, H reservoirs, respectively.

The number of atoms per unit area is fixed to three Au atoms per 5×1 unit cell according to the experimental findings for 0.6 ML coverage [5]. Also the number of H atoms is fixed. Therefore, it is convenient to study only relative formation energies $\Delta\Omega_f = \Omega_f - \Omega_f^{\mathrm{ref}}$ with respect to a reference surface with Ω_f^{ref} and $N_{\mathrm{Si}}^{\mathrm{ref}}$ for a varying chemical potential μ_{Si} of the Si reservoir, i.e.,

$$\Delta\Omega_f = E_{\mathrm{slab}}(N_{\mathrm{Si}}, N_{\mathrm{Au}}, N_{\mathrm{H}}) - E_{\mathrm{slab}}\left(N_{\mathrm{Si}}^{\mathrm{ref}}, N_{\mathrm{Au}}, N_{\mathrm{H}}\right) - \mu_{\mathrm{Si}} \Delta N_{\mathrm{Si}}, \tag{2}$$

where $\Delta N_{\mathrm{Si}} = N_{\mathrm{Si}} - N_{\mathrm{Si}}^{\mathrm{ref}}$ is the variation in the number of Si atoms. In all practical cases, we normalize $\Delta\Omega_f$ to a 5×2 surface. Because the substrate is bulk Si, we fix $\mu_{\mathrm{Si}} = -E_{\mathrm{tot}}^{\mathrm{Si}}$, with $E_{\mathrm{tot}}^{\mathrm{Si}}$ being the total energy of the Si diamond structure per atom. This value varies with the XC potential applied and the presence or absence of the spin polarization. Typical bulk energies vary in the interval $-E_{\mathrm{tot}}^{\mathrm{Si}} = 4.40$–$5.14$ eV given by the LDA and PBE functionals [19].

C. Electronic structure

The eigenvalues and eigenfunctions of the Kohn-Sham (KS) equation of the DFT [15] are used to describe the electronic structure. Generally, we discuss the results obtained with the PBE-GGA XC functional for the vdW-DF atomic geometries. Test calculations, however, show only a weak influence of the chosen XC functional on the electronic structure. The dispersion of not only the bulk Au and Si bands but also the surface bands is expected to be well described by the KS approximation [27]. However, since the excitation aspect is not considered in the DFT, the fundamental gap of Si is underestimated by about 100%. The shrinkage of the gap by about 0.5 eV has to be taken into consideration when discussing the position of surface states and comparing with experimental data. The underestimation of the gaps is the reason why we give STM images mainly for a bias voltage of ± 0.5 V, despite the fact that the majority of measured images have been observed for larger voltages, e.g., ± 1 V.

The Kohn-Sham results are also applied to compute electron densities and the energy-resolved local densities of states. The latter allow us to predict the bias dependence of the tunneling current in STM using the Tersoff-Hamann approach [28]. Following the majority of experimental STM studies, the

images are calculated for the constant-current mode [19]. The finite extent of the tunnel tip is taken into account. We simulate it by a Gaussian smoothing of the local density of states with a Gaussian of 1 Å at FWHM [29].

III. ATOMIC GEOMETRIES AND THEIR ENERGETICS

A. Models according to Erwin, Barke, and Himpsel

The construction of the EBH model [9] starts from the atomic geometry of the Si atoms in a bulk diamond structure with six-membered bond rings and atomic bilayers of Si tetrahedrons in the [111] direction. This EBH model is similar to the model proposed by Erwin for a Au coverage of 0.4 ML [6]. It is known that many metal substrates induce reconstructions based on silicon honeycomb (HC) chains in the [$\bar{1}$10] direction [3], i.e., ribbons of graphene-like arrangements of threefold-coordinated Si atoms in the plane. There structures may be identified as stripes of silicene [30–32]. However, in contrast to free-standing silicene, these layered structures are not buckled, in agreement with the original suggestions [9]. These Si HC chains are separated by a combination of a dimer row of Au atoms and a Au single row. The three structural elements result in the simple 5×1 reconstruction described by Fig. 1(a). With an additional dimerization within the Au double row, which results in an alternate rotation of the former Au dimers and a corresponding zigzag chain, the periodicity is doubled to 5×2 [see Fig. 1(b)]. The periodic decoration with Si adatoms in the region between the single and zigzag Au rows leads to additional reconstructions. In order to study the influence of adatoms, in general, we include one adatom per 5×4 unit cell [see Fig. 1(c)], in agreement with the adatom density favored in Ref. [9].

The relaxation of the three variations of the EBH model [9] displayed in Figs. 1(a), 1(b), and 1(c) gives rise to local minima on the total-energy surface independent of the used XC functional. The structural models shown in Fig. 1 are calculated using the vdW-DF method. The atomic coordinates only slightly depend on the applied functional, as shown in Table II. We only discuss a few characteristic parameters. Since the distances of the Au atoms in the chain direction are fixed to $d_{\mathrm{Si}} = \sqrt{2}a_0^{\mathrm{Si}}/2 = 3.86$ Å by the underlying bulk Si lattice with lattice constant a_0^{Si}, we focus on the Au double row with length D in the Au-Au bond in the [11$\bar{2}$] direction or slightly rotated against this direction. In order to characterize the rotation we measure the shorter and longer Au-Si distances d_1 and d_2 between Au atoms in a zigzag chain and a Si atom in the surface layer. In the case of the seemingly threefold-coordinated Si adatom for the 5×4 arrangement, we determine the bond length d_s to the Au atom of the single row also in the [11$\bar{2}$] direction. The bond lengths from the Si adatom to the two other adjacent Au atoms of the zigzag chain possess rather similar values. These parameters are listed in Table II. The bond length D in the double row is in the range of $D = 2.94$–2.96 Å. The values are similar to the Au distance in Au fcc bulk ($d_{\mathrm{Au}} = \sqrt{2}a_0^{\mathrm{Au}}/2 = 2.93$ Å for the vdW-DF method) and independent of rotations and adatoms. The Au-Si bond lengths $d_2 = 2.56$ Å and $d_s = 2.53$ Å for the case of the 5×4 unit cell are only slightly longer than the Au-Si bond lengths d_1 and d_2 for the case of 5×1 or 5×2 translation symmetry. These lengths are equal to or only somewhat longer than the sum of covalent radii (2.45 Å) for the two atoms [33]. This result can be interpreted as the observation of nearly covalent bonds of the Au double row to the Si surface and of the Si adatom to neighboring Au atoms.

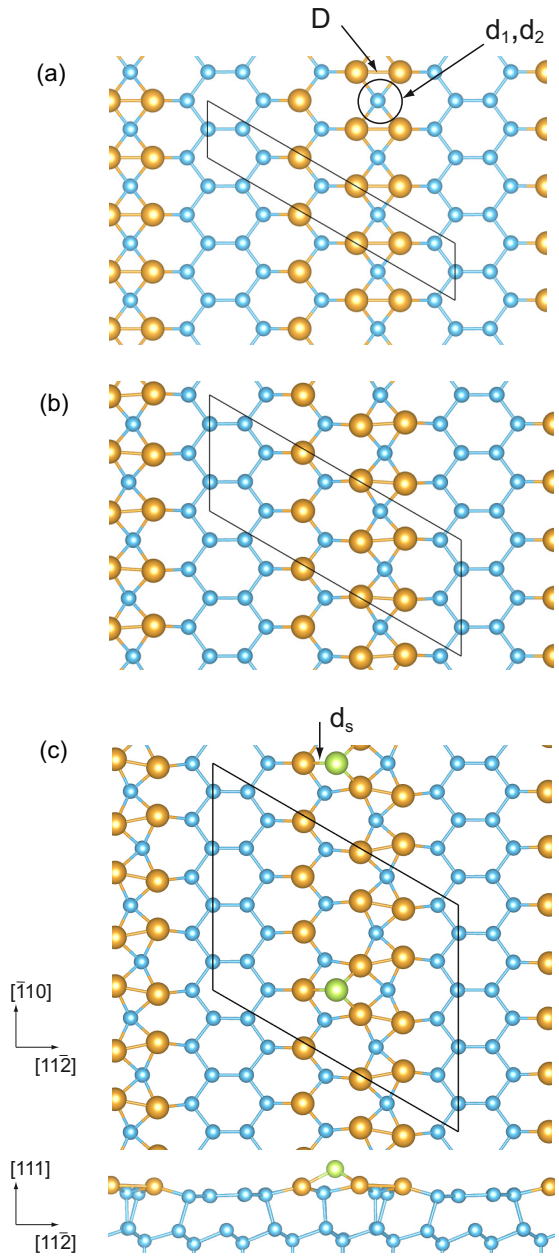

FIG. 1. (Color online) Calculated atomic structures proposed by the EBH model for a Si(111)-($5 \times n$)-Au surface with $n = 1,2,4$ and a Au coverage of 0.6 ML using the vdW-DF functional. (a) Top view of the EBH(5×1) model with ideal Au dimers. (b) Top view of the EBH(5×2) model. (c) Top and sides view of the EBH(5×4) model. The Si and Au atoms are displayed as light blue and yellow balls, respectively. The Si adatoms are represented as green balls. The surface unit cells are indicated by solid black lines. Characteristic geometry parameters (see text) are indicated.

The energetic orderings of the three studied variations of the EBH model are obvious from Table III. The energy difference

TABLE II. Characteristic bond lengths D, d_1, d_2, and d_s (see text) for the three different variations of the EBH model depicted in Fig. 1. The values are obtained by means of the vdW-DF method. The variation of the geometry parameters with the XC functionals is given in parentheses.

Model	D (Å)	d_1 (Å)	d_2 (Å)	d_s (Å)
EBH(5×1)	2.94 (2.88–2.97)	2.48 (2.43–2.49)	2.50 (2.46–2.42)	
EBH(5×2)	2.94, 2.95 (2.90–2.97)	2.46 (2.43–2.49)	2.51 (2.49–2.52)	
EBH(5×4)	2.94-2.96 (2.89–2.98)	2.47 (2.44–2.48)	2.56 (2.53–2.56)	2.53 (2.50–2.54)

between the 5×1 and 5×2 symmetries is small. However, the geometrical model with the 5×4 unit cell with one additional Si adatom is energetically more stable with respect to the basic EBH model with a 5×1 or 5×2 unit cell without the Si adatom. Thus, the Si adatom further stabilizes the zigzag double rows over an ideal ladderlike arrangement of Au-Au bonds in the $[\bar{1}10]$ chain direction. The general tendencies are independent of the XC functional used. Only the magnitude of the energy gain and the deformation of the Au double rows are influenced. Our results of the relative surface energies are in close agreement with other DFT findings employing the LDA, PBE, or PBEsol XC functional [13].

Adatoms may influence the atomic geometry and the energetics, especially the dimerization of the Au chains [9,12,34–37]. Following Erwin *et al.* [9], we investigate the strength of the dimerization, particularly the influence of XC functionals on it. The results are summarized in Fig. 2. We introduce a relative dimerization parameter by measuring the larger distance d of two such atoms closer to the Si honeycomb chain with respect to the nonrotated situation $d_{\mathrm{Au}} = \sqrt{2}a_0^{\mathrm{Au}}/2$ by $\Delta = (d - d_{\mathrm{Au}})/d_{\mathrm{Au}}$. In Fig. 2(a) we illustrate the effect of the chosen XC functional on the dimerization between Au atoms of two different rungs of the ladder parallel to the $[\bar{1}10]$ direction without adatoms. For the (5×2) model the curves versus the dimerization are symmetric, in agreement with the surface symmetry. The parameter Δ minimizing the total energy is also listed in Table III. It exhibits the significant effect of the XC functionals. We find that without adatoms the dimerization vanishes for the PBE-GGA functional and remains small for the vdW-DF method. Surprisingly, both the PBEsol and LDA functionals give rise to a significant dimerization. With an adatom in the system [Fig. 1(c)], we find a significant stabilization of a positive dimerization, as shown in Fig. 2(b). The dimerization parameters Δ of the reconstructed EBH(5×4) model are also listed in Table III and are of the order of 0.15. In the case of (5×4) periodicity we find that the dimerization parameter is rather independent of the XC functional used. Only the accompanying energy gain is influenced by the XC functional. A comparison of the energy gains indicates that a significant contribution to the stabilization of the surface geometry by adatoms is due to additional electrons which are donated by the Si adatom and fill electronic states that are empty in the adatom-free case.

B. Models according to Abukawa and Nishigaya

The recently reported AN model [10] suggests the arrangement of the six Au atoms per 5×2 unit in an Eiffel Tower–like arrangement oriented in the $[11\bar{2}]$ direction. Such arrangements are in agreement with the Y-shaped structures found in STM images [11,12]. However, this arrangement requires structural motifs of the Si and Au atoms completely different from the honeycomb chains and ladderlike structures in the EBH model. The AN model contains undercoordinated Si atoms arranged in the $[\bar{1}10]$ direction parallel to the zigzaglike Au chains, and Si honeycomb chains are absent, which is also a different structural motif than those found in the EBH model. Structural elements such as hollows and seven-member ring structures connecting Si and Au atoms appear in the original model [10]. However, the atomic relaxation shows that the original AN model [10] is unstable because of energetically unfavorable structural elements such as seven-member rings and undercoordinated Si atoms (see also Ref. [13]).

The originally proposed AN model with AN(5×2) translational symmetry decays and transforms barrierless in a new geometry that we call AN(5×2)a [see Fig. 3(a)]. The new geometry has the six-member ring structure and highly coordinated Si atoms surrounded by three Au atoms. After taking away one highly coordinated Si surface atom surrounded by three Au atoms in the AN(5×2)a geometry, the surface structure relaxes into a new adatom-free structure with a 5×2 unit cell [henceforth called AN(5×2)b; see Fig. 3(b)]. The Si coverage of the AN(5×2)b geometry is the same as that of the basic EBH model with a 5×2 unit cell in Fig. 1(b). Just as in the case of the EBH model we can consider a (5×4)

TABLE III. The formation energy $\Delta\Omega_f$ in Eq. (2) for different variations of the EBH and AN models calculated by means of different XC functionals (see text). The energies are given in units of eV/(5×2 unit cell) with respect to the EBH(5×2) structure. In the case of the reconstructed EBH models with 5×2 and 5×4 periodicities the relative dimerization parameter Δ is also listed in parentheses. It results from a minimization of the Hellmann-Feynman forces.

XC functional	EBH(5×1)	EBH(5×2)	EBH(5×4)	AN(5×2)a	AN(5×2)b	AN(5×4)
LDA	0.06	0.00 ($\pm$0.15)	$-$0.25 (0.17)	1.14	0.92	0.86
PBE-GGA	0.00	0.00 ($\pm$0.00)	$-$0.12 (0.13)	1.38	0.84	0.89
PBEsol	0.03	0.00 ($\pm$0.12)	$-$0.24 (0.16)	1.06	0.89	0.83
vdW-DF	0.00	0.00 ($\pm$0.05)	$-$0.16 (0.15)	1.42	0.82	0.86

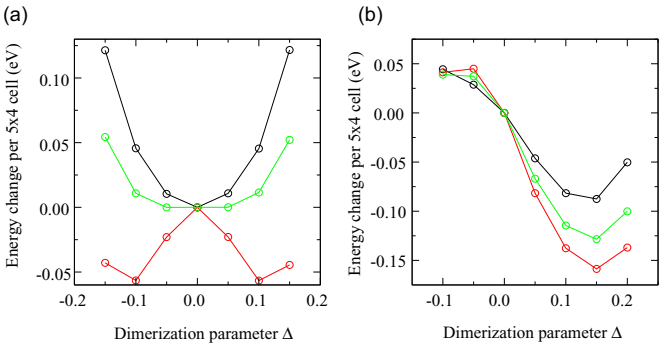

FIG. 2. (Color online) Energy variation vs the dimerization parameter of Au atoms in (a) the EBH(5 × 2) model without adatom and (b) the EBH (5 × 4) model with one adatom for three different XC functionals: PBE-GGA (black), PBEsol (red), and vdW-DF (green).

reconstruction with one Si adatom above the center of each second six-member ring based on the AN(5 × 2)b model [see Fig. 3(c)]. In the analysis of the geometrical properties we focus on the most important distance between neighbored Au atoms. We characterize such an AN-derived geometry by three atomic distances. Two vertical distances are parallel to the $[\bar{1}10]$ direction of two Au atoms in the zigzaglike chain, D_a, which can be influenced by an additional Si atom, and D_w, which is farther away from such a Si atom but is closer to the Au pair; the third, D_p, is the distance of the two Au atoms in the pair oriented parallel to the $[11\bar{2}]$ direction. For the AN-derived (5 × 4) model we also determine the bond length d_s of the Si adatom to the Au atom of the single row in the $[11\bar{2}]$ direction as in the EBH case. The resulting values are listed in Table IV.

In general, all relaxed vertical atomic positions (not shown in Table IV) differ substantially from those predicted by RHEED [10]. The relaxed Y-shaped structures seemingly cannot explain the data derived within the structural studies. The lateral distances depend on the density of the Si adatoms, as indicated by a comparison of Figs. 3(a), 3(b), and 3(c). The comparison of the densities explains how the distances D_a and D_w of two Au atoms in the $[\bar{1}10]$ direction deviate from their mean value $d_{\mathrm{Si}} = \sqrt{2}a_0^{\mathrm{Si}}/2 = 3.86$ Å (for vdW-DF), which is fixed by the underlying Si substrate. Also, the distance D_p of the atoms in a Au pair varies with the presence or absence of an adjacent Si adatom. However, D_p is smaller than the Au-Au dimer bond length D of the EBH model. It is only slightly longer than the sum (2.68 Å) of the covalent radii of two Au atoms [33], thereby indicating an almost covalent bond between them. Here we find that the Au-Au pairs in the AN-derived relaxed models have a different orientation than those in the model originally proposed by Abukawa and Nishigaya [10]. The AN-derived models which we optimized here are not consistent with the bonding orientation suggested by the experimental results in [10]. The substantial variations of the Au-Au distances D_w along the $[\bar{1}10]$ direction in the case of Fig. 3(c) indicate again the strong influence of the adatoms on the Au dimerization. The bond length d_s from the Si adatom to a Au atom in the topmost layer is 2.57 Å. This value is similar the value of 2.53 Å for the distance in the EBH(5 × 4) model geometry listed in Table II.

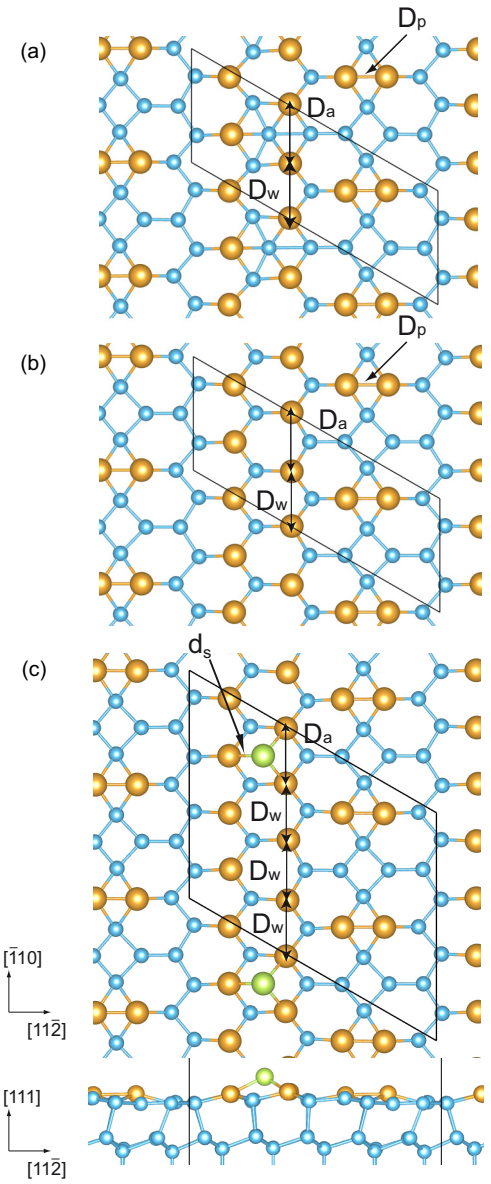

FIG. 3. (Color online) Calculated atomic structures derived from the surface model originally proposed by Abukawa and Nishigaya [10] for a gold coverage of 0.6 ML using the vdW-DF functional. The Si and Au atoms are displayed as light blue and yellow balls, respectively. The Si adatoms are displayed as green balls. The surface unit cells are indicated by solid black lines. (a) Top view of the relaxed AN(5 × 2) model with the resulting six-member rings and filled hollows [AN(5 × 2)a]. (b) Top view of the adatom-free AN(5 × 2) model [AN(5 × 2)b]. (c) Top and side views of the AN(5 × 4) model with one adatom.

The changes in the formation energy $\Delta\Omega_f$ with respect to the EBH(5 × 2) model in Table III clearly show that the AN model is energetically unfavorable. An atomic arrangement according to the AN reconstruction cannot occur in thermodynamic equilibrium. The energy loss of about 0.1 eV/(1 × 1 unit cell) indicates that thermal effects cannot stabilize an AN-derived structure. We clearly state that an AN-derived model cannot occur under equilibrium conditions. However, within the AN models there are also drastic differences among

TABLE IV. Characteristic distances D_a, D_w, D_p, and d_s (see text) for three different derivatives of the AN model depicted in Fig. 3. The values are listed for the two 5×2 translational symmetries, AN(5×2)a and AN(5×2)b (see text). In addition, values for a 5×4 structure with one Si adatom [AN(5×4)] are given. In the last case the three D_w values vary with distance to the Si atoms and Au pairs, and two D_p values are given for pairs closer to and more distant from the adatom, respectively. The values are obtained by means of the vdW-DF method. The variation of the geometries with the various XC functionals is given in parentheses.

Model	D_a (Å)	D_w (Å)	D_p (Å)	d_s (Å)
AN(5×2)a	4.02 (3.96–4.02)	3.69 (3.68–3.71)	2.77 (2.73–2.79)	
AN(5×2)b	4.00 (3.93–4.00)	3.71 (3.64–3.80)	2.82 (2.77–2.85)	
AN(5×4)	3.73 (3.73–3.76)	3.78, 4.10, 3.82 (3.72–4.10)	2.82, 2.83 (2.77–2.85)	2.57 (2.42–2.48)

their formation energies. True adatoms on top of the surface six-member ring [see Fig. 3(c)] do not significantly influence the surface energetics. The AN(5×2)b structure found after relaxation of the starting AN(5×2)a model with six-member rings and filled hollow regions [Fig. 3(b)] is much more stable than that with seven-member rings [Fig. 3(a)]. Consequently, the electronic structure of the AN(5×2)a model will not be investigated in the following section.

IV. ELECTRONIC STRUCTURE

A. STM images

Measured STM images of the Au-coverage Si(111) surface [9,11–13,38,39] show bright rows along the [$\bar{1}$10] direction which are separated by (mostly) thinner dark regions. They usually show a ($\times$4) or ($\times$2) periodicity at their edge, which can be compared with images simulated for 5×4 or 5×2 reconstructions. The rows contain elongated Y-shaped elements or smaller V-shaped ones. Many of the STM images exhibit bright spots in the rows independent of the tunnel bias. The simulated STM images are displayed in Fig. 4 for the 5×4 adatom geometries of both basic models, EBH and AN. Many of the mentioned key features such as bright rows, dark regions in between rows, and some bright spots are visible independent of the EBH or AN model. In any case, the dominating role of the adatoms in STM images is clearly visibly in Fig. 4 for both empty-state and filled-state images, in agreement with other findings [9].

The differences in the rows are much more visible in the simulated images in Fig. 5 for the EBH(5×2) and AN(5×2)b surface structures without Si adatoms. Still, the [$\bar{1}$10]-oriented gold chains independent of the arrangement of the Au atoms dominate the bright rows. However, their details vary with the bias sign and the basic model. The rows for EBH(5×2) in Fig. 5(a) clearly exhibit the Y-shaped elements for negative bias. For positive voltage such elements are still available but are difficult to distinguish from V-shaped elements. In any case the bright rows are separated by dark rows corresponding to the honeycomb chains. Only their width varies with the sign of the bias voltage.

In the case of the relaxed AN(5×2)b model the images in Fig. 5(b) are completely different. In the case of negative bias the occurrence of Y-shaped elements cannot be excluded. However, the dark regions between the rows do not form channels with a defined width. Rather, they are sometimes narrowed or even interrupted by bright spots. For large positive bias the effect of the gold atoms disappears, particularly for +1 V (not shown in Fig. 5). In summary, in studying the finer structure of the images of the AN model it becomes clear that this basic model cannot successfully explain the details of the experimentally observed images, even though the originally predicted towerlike structural motifs are related to the Y-shaped features found in STM images.

B. Energy bands and density of states

In order to compare the electronic structures of the EBH and AN models we focus on the 5×4 geometries with one Si adatom per surface unit cell, as shown in Figs. 1(c) and 3(c). Adatoms have been seen in practically all STM images, as

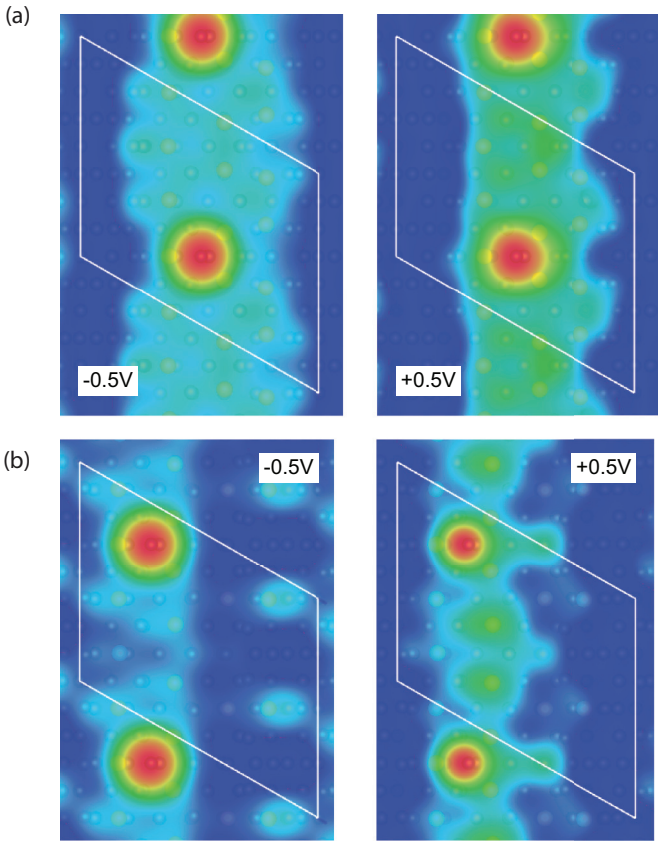

FIG. 4. (Color online) Simulated STM images for bias voltages of $\pm$0.5 V for (a) the EBH(5×4) and (b) AN(5×4) adatom models. Red (blue) indicates the highest (lowest) tunnel probability. The unit cell is indicated.

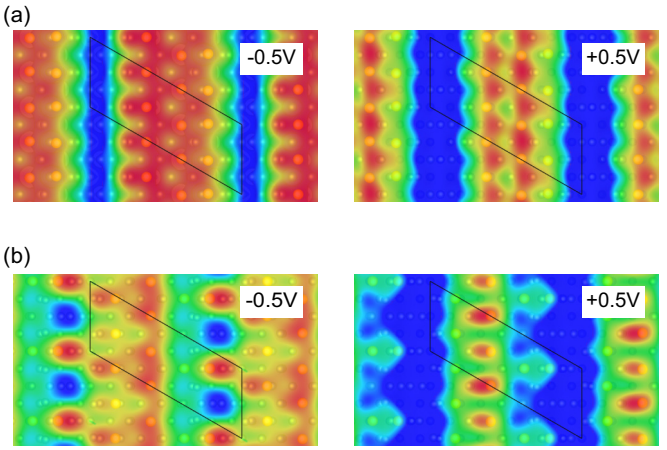

FIG. 5. (Color online) Simulated STM images for bias voltages of ± 0.5 V for the adatom-free, relaxed (a) EBH(5×2) and (b) AN(5×2)b geometries. The highest (lowest) tunneling probability is indicated in red (blue). The surface unit cell is indicated by thin black lines.

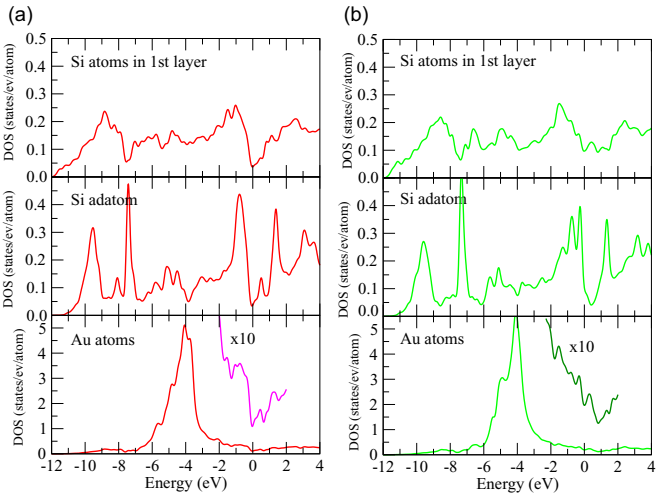

FIG. 7. (Color online) Surface-sensitive one-electron density of states projected onto atoms in the uppermost Si atomic layer, the Si adatom, and the Au atoms for (a) EBH(5×4) and (b) AN(5×4). The Fermi level is taken as zero energy. In the case of Au the DOS around zero energy is increased by a factor of 10.

we discussed above. First, we study the band structures of the chosen slabs along the [11$\bar{2}$] high-symmetry line in the surface BZ up to the BZ boundary A_4 in Fig. 6. For a better understanding of the contributions of the surface, the densities of states projected onto the Si atoms in the uppermost atomic layer, the Si adatom, and the Au atoms are depicted in Fig. 7.

The band structures in Fig. 6 show some general features which are common for the two basic models of Au-covered surfaces. The Fermi levels of the slab systems appear close to the valence-band maximum of bulk silicon. Consequently, several empty surface bands appear in the projected fundamental gap of bulk Si, whose character will be discussed below. Occupied and empty surface bands also appear near the Fermi level. An indirect but almost vanishing gap occurs for AN(5×4), with a minimum of the empty surface band near $\Gamma A_4/3$. Within the Kohn-Sham approach and neglecting

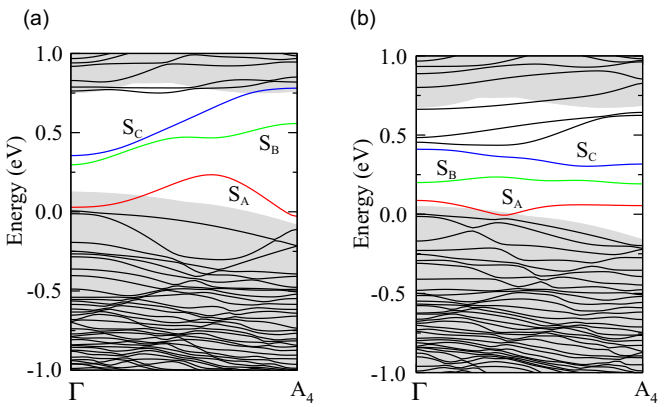

FIG. 6. (Color online) Calculated energy bands of Si(111)-(5×4)-Au for the adatom geometries based on the (a) EBH and (b) AN models. The Fermi level is taken as zero energy. The projected bulk Si band structure is displayed as gray areas. The average electrostatic potentials in the slab center and of the bulk Si are used for alignment. The three lowest empty surface bands are labeled by S_A, S_B, and S_C.

the spin-orbit interaction, the EBH(5×4) surface represents a half metal due to the occupation of the band S_A near the BZ boundary A_4. We qualitatively agree with Erwin *et al.* [9] that having one Si adatom per 5×4 unit cell creates a multiband metal-insulator transition on the Si(111)-(5×2)-Au surface. The perturbation due to the adatom lifts the band degeneracy at the BZ boundary (not shown). Together with the resulting band filling, a surface gap appears between the uppermost occupied slab band and the empty S_A band. This gap opening, which is one of the reasons for the surface stabilization by Si adatoms, is in agreement with findings of earlier ARPES measurements [34,35].

It is difficult to compare the uppermost occupied bands in Figs. 6(a) and 6(b) directly with ARPES measurements of the adatom-doped Si(111)-(5×2)-Au surface [9,12,34,35]. One reason is the use of the BZ of the 5×4 surface translational symmetry. In comparison to the number of bands in the 5×2 surface the number of bands in the 5×4 surface is doubled by the band folding and is additionally slightly modified by the adatoms, as discussed above. Keeping the folding argument in mind, the increase in the experimentally found band from small wave vectors to that around A_4 can be explained by a second occupied band (near the first A_4 band) in Fig. 6(a). The uppermost occupied band may be related to the downward bended measured band for wave vectors between A_4 and the BZ boundary of the 5×2 surface along the [11$\bar{2}$] direction. However, a quantitative comparison also requires the inclusion of spin-orbit coupling and perhaps quasiparticle effects. In any case, it seems to be impossible to make such a qualitative explanation based on the dispersion of the uppermost occupied bands of the AN model in Fig. 6(b). This fact again raises the doubts concerning the validity of AN-derived models.

In contrast to the occupied bands the empty surface bands have been investigated only indirectly by a few empty-state STM images. Here we perform such investigations

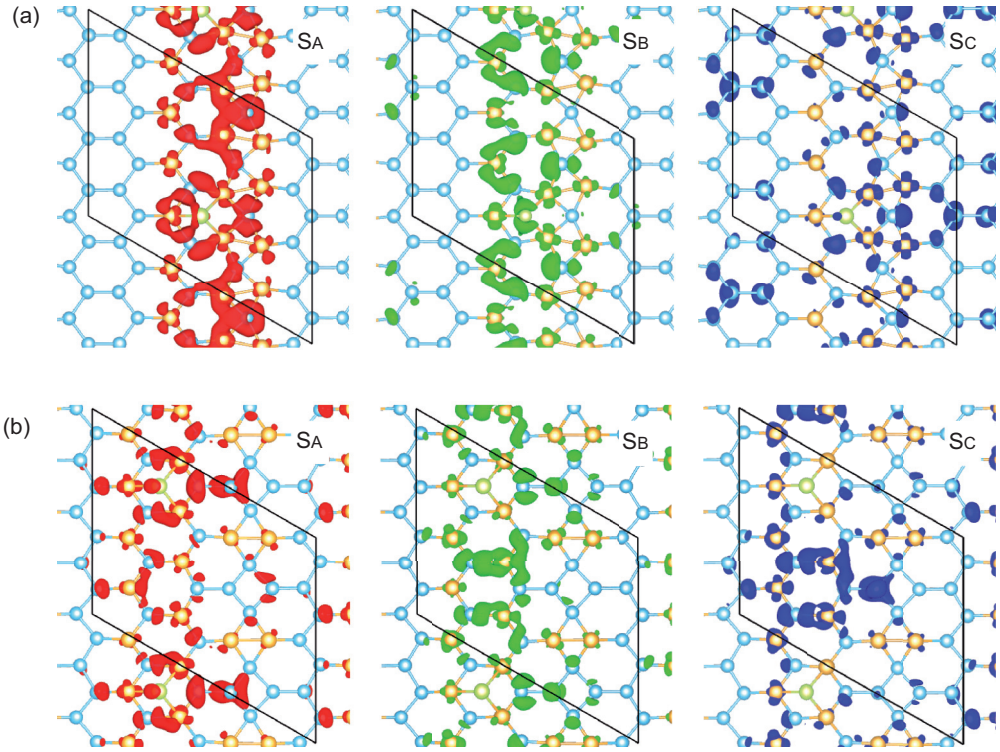

FIG. 8. (Color online) Wave-function squares of the three lowest empty surface bands S_A, S_B, and S_C for the (a) EBH(5×4) and (b) AN(5×4) models. The partial-charge-density isosurface is shown up to 1.0×10^{-3} $e/\text{Å}^3$. The Si atoms, Au atoms, and Si adatoms are displayed as blue, yellow, and light green circles, respectively. The 5×4 unit cell is indicated by black solid lines.

energetically, by means of the projected density of states in Fig. 7, and spatially, by the probability of finding an electron near the Fermi level as presented in Fig. 8. The DOS spectra in Fig. 7 projected onto the 24 Si atoms in the uppermost surface layer, the single Si adatom on top, and the 12 Au atoms in the 5×4 surface unit cell are rather similar in the entire energy region considered. The major differences appear in the Si-derived spectra near the Fermi energy. The disappearance of the honeycomb chains in the AN model gives rise to a high density of states near the Fermi level [see Fig. 7(b), top panel]. This is in contrast to the strong reduction near the Fermi level for the EBH model. Its line shape resembles the linear variation of the DOS of a complete Si honeycomb sheet, the freestanding silicene [30–32]. The adatom-related DOS shows a splitting of the highest occupied part in the AN model. The most interesting feature, however, is the occurrence of an adatom-related peak 0.5 eV above the Fermi level in the EBH case [see Fig. 7(a), middle panel]. Differences between the two surface models in the Au-projected DOS are hardly visible. The DOS is dominated by a band due to the localized Au $5d$ electrons with a peak maximum near -4 eV. Around the Fermi level the arrangement of the Au atoms and hence the bonding behavior of the Au $6s$ electrons only play a minor role. The spectra in Fig. 7 cannot directly be compared with measurements. Yoon *et al.* [12] published site-dependent scanning tunneling spectra (dI/dV) on top of an adatom and also on different positions of the bright rows seen in the filled-state images in Fig. 5. Since the adatom density is not known, the definition of a joint energy zero of the experimental spectra [12] and the theoretical ones in Fig. 7 is difficult. Nevertheless, the four-peak structure around the Fermi level found for the adatom position in the energy interval (-1 eV, $+1$ eV) with the highest intensities of the most distant peaks also occurs in the theoretical DOS for the EBH model, indicating the fact that adatoms influence the spectrum around the Fermi level but are dependent on their bonding arrangement.

The enormous role of the Au atoms in the formation of the three lowest empty bands in Fig. 6 is illustrated by the wave-function squares in Fig. 8. They are averaged over the entire BZ. In the EBH case [Fig. 8(a)] the two lowest states are dominated by Au atoms and their bonding to adjacent Si atoms. While the lowest band is dominated by the intermediate vertical Au chain, the probability of finding an electron is mainly localized in the single Au row bonded to the Si honeycomb chain. In the first case, states at Si atoms between two Au rings also contribute. In the second case contributions from the Si adatom are observable. The quasi-one-dimensional character of the S_A and S_B states is very interesting and is clearly visible in Fig. 8(a). There is no interaction across the honeycomb chains and with the substrate. Therefore, the two lowest empty bands should give us the opportunity to demonstrate features of 1D physics. The wave function of the third empty S_C band possesses Au and Si contributions. Therefore, the contributions from Si atoms between the rungs and in the honeycomb chains near the Si adatom are most pronounced. In the case of the AN model [Fig. 8(b)] the Au-Si and Si-Si bonds seem to play a stronger role. For the lowest S_A band such contributions near the adatom are the most important ones, whereas for the Au-Si bond the bands

that are in the tower basis but away from the adatom give the strongest contributions. In any case the lowest two empty S_A and S_B bands are more Au related for the EBH geometry than for the AN geometry.

V. SUMMARY AND CONCLUSIONS

In summary, we have performed *ab initio* investigations in the framework of the density-functional theory of geometric and electronic structures of Si(111)-(5 × 2)-Au and adatom-doped Si(111)-(5 × 4)-Au surfaces. We found some principal results for the geometries and their energetics: (i) The use of a certain exchange-correlation functional only qualitatively influences the results. Only the dimerization of the Au double row depends on the choice of the XC. (ii) Si adatoms, at least for a decoration of two 5 × 2 cells with one adatom, stabilize the EBH structure but do not stabilize the AN structure by any means. (iii) The original geometry proposed by Abukawa and Nishigaya transforms barrierless in a surface structure without seven-member rings and filled hollow sites. (iv) Energetically, the EBH model is clearly favored over the relaxed AN one. Taking this result together with the occurrence of Si adatoms in experimental studies we conclude that the EBH model explains the distribution of Au atoms over the surface much better than the AN model.

The results for the electronic structures are less conclusive in discriminating the two basis models, EBH and (relaxed) AN. Bright spots indicating adatoms in STM images can be described in both models. Significant differences appear for the empty-state STM images. The bright rows observed experimentally do not occur in the calculated images of AN(5 × 2)b. Concerning the uppermost filled surface bands measured by means of ARPES, the band predictions of the presented theory without spin-orbit coupling and quasiparticle effects in the 5 × 4 BZ are not conclusive. In terms of bands in an extended zone scheme the observed band dispersion seems to be explained by means of the EBH model. Wave functions of the first layer of Si atoms, the Au decoration, and Si adatoms contribute to the electronic structure around the Fermi level independent of the applied surface model. The most striking difference seems to be the occurrence or disappearance of the Si honeycomb chains. In any case, it becomes clear that the potential of theoretical and experimental studies of the empty surface states has not been exhausted until now. Further studies are also required to understand better the quasi-one-dimensional character of the lowest empty surface bands.

ACKNOWLEDGMENTS

We acknowledge financial support from the Deutsche Forschungsgemeinschaft (Germany) through the research unit FOR1700 (Grant No. Be1346/21-1). A grant of computer time from the John von Neumann Institute for Computing (NIC) in Jülich is also gratefully acknowledged.

[1] S. Hasegawa, J. Phys. Condens. Matter **12**, R463 (2000).
[2] I. Matsuda and S. Hasegawa, J. Phys. Condens. Matter **19**, 355007 (2007).
[3] P. C. Snijders and H. H. Weitering, Rev. Mod. Phys. **82**, 307 (2010).
[4] H. E. Bishop and J. C. Rivière, J. Phys. D **2**, 1635 (1969).
[5] I. Barke, F. Zheng, S. Bockenhauer, K. Sell, V. v. Oeynhausen, K. H. Meiwes-Broer, S. C. Erwin, and F. J. Himpsel, Phys. Rev. B **79**, 155301 (2009).
[6] S. C. Erwin, Phys. Rev. Lett. **91**, 206101 (2003).
[7] S. Riikonen and D. Sánchez-Portal, Phys. Rev. B **71**, 235423 (2005).
[8] F.-C. Chuang, C.-H. Hsu, C.-Z. Wang, and K.-M. Ho, Phys. Rev. B **77**, 153409 (2008).
[9] S. C. Erwin, I. Barke, and F. J. Himpsel, Phys. Rev. B **80**, 155409 (2009).
[10] T. Abukawa and Y. Nishigaya, Phys. Rev. Lett. **110**, 036102 (2013).
[11] J. D. O'Mahony, C. H. Patterson, J. F. McGilp, F. M. Leibsle, P. Weightman, and C. F. J. Flipse, Surf. Sci. **277**, L57 (1992).
[12] H. S. Yoon, J. E. Lee, S. J. Park, I.-W. Lyo, and M.-H. Kang, Phys. Rev. B **72**, 155443 (2005).
[13] C. Hogan, E. Ferraro, N. McAlinden, and J. F. McGilp, Phys. Rev. Lett. **111**, 087401 (2013).
[14] P. Hohenberg and W. Kohn, Phys. Rev. **136**, B864 (1964).
[15] W. Kohn and L. J. Sham, Phys. Rev. **140**, A1133 (1965).
[16] G. Kresse and J. Furthmüller, Comput. Mater. Sci. **6**, 15 (1996).
[17] J. P. Perdew and A. Zunger, Phys. Rev. B **23**, 5048 (1981).
[18] J. P. Perdew, K. Burke, and M. Ernzerhof, Phys. Rev. Lett. **77**, 3865 (1996).
[19] S. Sauer, F. Fuchs, F. Bechstedt, C. Blumenstein, and J. Schäfer, Phys. Rev. B **81**, 075412 (2010).
[20] J. P. Perdew, A. Ruzsinszky, G. I. Csonka, O. A. Vydrov, G. E. Scuseria, L. A. Constantin, X. Zhou, and K. Burke, Phys. Rev. Lett. **100**, 136406 (2008).
[21] M. Dion, H. Rydberg, E. Schröder, D. C. Langreth, and B. I. Lundqvist, Phys. Rev. Lett. **92**, 246401 (2004).
[22] J. Klimeš, D. R. Bowler, and A. Michaelides, Phys. Rev. B **83**, 195131 (2011).
[23] G. Kresse and D. Joubert, Phys. Rev. B **59**, 1758 (1999).
[24] H. J. Monkhorst and J. D. Pack, Phys. Rev. B **13**, 5188 (1976).
[25] A. E. Mattsson, R. Armiento, J. Paier, G. Kresse, J. M. Wills, and T. R. Mattsson, J. Chem. Phys. **128**, 084714 (2008).
[26] F. Bechstedt, *Principles of Surface Physics* (Springer, Berlin, 2003).
[27] W. Aulbur, L. Jönsson, and J. Wilkins, *Quasiparticle Calculations in Solids, in Solid State Physics: Advances in Research and Applications*, edited by H. Ehrenreich and F. Spaepen (Academic Press, San Diego, 1999), Vol. 54, pp. 1–218.
[28] J. Tersoff and D. R. Hamann, Phys. Rev. B **31**, 805 (1985).
[29] E. J. Snyder, E. A. Eklund, and R. S. Williams, Surf. Sci. **239**, L487 (1990).
[30] S. Cahangirov, M. Topsakal, E. Aktürk, H. Şahin, and S. Ciraci, Phys. Rev. Lett. **102**, 236804 (2009).
[31] A. Kara, H. Enriquez, A. P. Seitsonen, L. C. Lew Yan Voon, S. Vizzini, B. Aufray, and H. Oughaddou, Surf. Sci. Rep. **67**, 1 (2012).

[32] L. Matthes, P. Gori, O. Pulci, and F. Bechstedt, Phys. Rev. B **87**, 035438 (2013).
[33] Sargent-Welch, *Table of Periodic Properties of the Elements* (Skokie, IL, 1980).
[34] J. L. McChesney, J. N. Crain, V. Pérez-Dieste, F. Zheng, M. C. Gallagher, M. Bissen, C. Gundelach, and F. J. Himpsel, Phys. Rev. B **70**, 195430 (2004).
[35] W. H. Choi, P. G. Kang, K. D. Ryang, and H. W. Yeom, Phys. Rev. Lett. **100**, 126801 (2008).
[36] E. Bussmann, S. Bockenhauer, F. J. Himpsel, and B. S. Swartzentruber, Phys. Rev. Lett. **101**, 266101 (2008).
[37] I. Barke, S. Polei, V. v. Oeynhausen, and K.-H. Meiwes-Broer, Phys. Rev. Lett. **109**, 066801 (2012).
[38] A. Kirakosian, J. Crain, J.-L. Lin, J. McChesney, D. Petrovykh, F. Himpsel, and R. Bennewitz, Surf. Sci. **532-535**, 928 (2003).
[39] S. Polei, I. Barke, S. C. Erwin, and K.-H. Meiwes-Broer, Phys. Rev. B **85**, 165414 (2012).